

A study of the 1/2 retrograde resonance

Periodic orbits and resonant capture

M.H.M. Morais · F. Namouni · G. Voyatzis · T.
Kotoulas

Received: date / Accepted: date

Abstract We describe the families of periodic orbits in the 2-dimensional 1/2 retrograde resonance at mass ratio 10^{-3} , analyzing their stability and bifurcations into 3-dimensional periodic orbits. We explain the role played by periodic orbits in adiabatic resonance capture, in particular how the proximity between a stable family and an unstable family with a nearly critical segment, associated with Kozai separatrices, determines the transition between distinct resonant modes observed in numerical simulations. Combining the identification of stable, critical and unstable periodic orbits with analytical modeling, resonance capture simulations and computation of stability maps helps to unveil the complex 3-dimensional structure of resonances.

Keywords Resonance. Three-body problem.

1 Introduction

The study of retrograde resonances in the restricted 3-body problem was initiated in Morais & Giuppone (2012); Morais & Namouni (2013b) with later developments by Morais & Namouni (2016a); Namouni & Morais (2018c, 2020b). There are now examples of retrograde resonances in the Solar System for the period ratios 1/2 and 2/5 with Jupiter (Centaur 330759) 2008 S0218 and 2006 BZ8), 2/3 with Saturn (Centaur 2009 QY6) (Morais & Namouni, 2013a) and 1/1 with Jupiter (asteroid (514107) Ka'epaoka'awela) (Morais & Namouni, 2017; Wiegert et al., 2017) and such configurations are likely to exist in extrasolar systems (Gayon & Bois, 2008; Gayon-Markt & Bois, 2009; Li et al., 2019). Additionally,

M. H. M. Morais, Instituto de Geociências e Ciências Exatas, Universidade Estadual Paulista (UNESP), Av. 24-A, 1515 13506-900 Rio Claro, SP, Brazil

F. Namouni
Université Côte d'Azur, CNRS, Observatoire de la Côte d'Azur, CS 34229, 06304 Nice, France

G. Voyatzis
Aristotle University of Thessaloniki, Department of Physics, 54124, Thessaloniki, Greece

T. Kotoulas
Aristotle University of Thessaloniki, Department of Physics, 54124, Thessaloniki, Greece

high inclination and retrograde orbits currently orbiting our Sun may be of interstellar origin (Namouni & Morais, 2018a, 2020a) hence the study of high inclination and retrograde resonances is necessary to understand how these could be captured by the Solar System.

The numerical study on resonance capture at arbitrary inclination by Namouni & Morais (2015, 2017, 2018b) showed that retrograde resonances capture more efficiently than prograde resonances and that this effect is more pronounced for the 1/1 and 1/2 retrograde resonances. Moreover, a 3-phase capture mechanism for retrograde resonances was observed in the numerical simulations by Namouni & Morais (2015); Morais & Namouni (2016a). The observed capture stages consist of: 1) libration of the prograde resonant angle at small eccentricity; 2) Kozai resonance with coupled eccentricity and inclination oscillations where both prograde and retrograde resonant angles librate; 3) exit of the Kozai resonance and libration of the retrograde resonant angle.

Computation of periodic orbits (POs) is a powerful tool to unveil the phase space structure in conservative dynamical systems. In the planar circular restricted 3-body problem (CR3BP), the motion occurs in a 3-dimensional surface embedded in the 4-dimensional phase space. A 2-dimensional section of this surface is called a Poincaré map and POs are fixed points on this map which may be stable or unstable. When there is a dominant central mass (e.g. the case Sun-planet-asteroid), stable POs correspond to nearly circular orbits or exact resonances between the asteroid and planet's orbital frequencies, while unstable POs correspond to separatrices which delimit the regions of quasiperiodic motion around stable POs. In the spatial CR3BP, the motion occurs on a 5-dimensional surface embedded in the 6-dimensional phase space thus Poincaré maps are not useful as a visualization tool. However, the families of stable and unstable POs may still be computed providing information about the resonances in the 3-dimensional (3D) problem.

Until recently, most 3D searches were performed for prograde motion (inclination less than 90°) e.g. in Voyatzis et al. (2018) and Antoniadou & Voyatzis (2014), based on continuation of planar prograde POs. The few searches which were extended to retrograde motion (inclination larger than 90°) were also based on continuation of planar prograde POs (Kotoulas & Voyatzis, 2005; Antoniadou & Libert, 2019). Morais & Namouni (2019) computed for the 1st time the families of stable POs for the planar retrograde 1/1 resonance and obtained the spatial families which bifurcate from them. Subsequently, Kotoulas & Voyatzis (2020a) computed the families of planar POs for interior retrograde resonances with Jupiter (i.e. with semimajor axis smaller than the planet's) and more recently the same authors computed the families of 3-dimensional symmetric POs for the exterior 1/2, 2/3 and 3/4 resonances with Neptune (i.e. with semimajor axis larger than the planet's) based on continuation from planar prograde and retrograde POs (Kotoulas & Voyatzis, 2020b). Morais & Namouni (2019) explained how the families of POs for the retrograde 1/1 resonance determine resonant capture, in particular the 3-phase mechanism observed in the simulations (Namouni & Morais, 2015; Morais & Namouni, 2016a). The purpose of the current article is to extend the study of Morais & Namouni (2019) to the exterior 1/2 retrograde resonance, focusing on explaining the 3-phase capture mechanism and on unveiling the resonance structure associated with the PO families. This has not been addressed in previous studies.

We performed a search of periodic orbits for the retrograde 1/2 resonance in the CR3BP at mass ratio $\mu = 10^{-3}$ following the methodology described in Sect. 2. In Sect. 3 we describe the families that exist in the 2D problem and their bifurcations to the 3D problem. In Sect. 4 we show examples of adiabatic capture in resonance, the connection with the periodic orbit (PO) families computed previously and predictions from analytical models. The conclusions of this study are presented in Sect. 5.

2 Computation of periodic orbits

Periodic orbits (POs) of period T satisfy the periodicity conditions $\bar{X}(\bar{X}_0, T) = \bar{X}_0$ where $X = (x, z, \dot{x}, \dot{y}, \dot{z})$ is the phase space vector on the surface of section $y = 0$. POs are associated with resonances and may be classified as symmetric, when the critical angle is 0 or 180° , or asymmetric, when the critical angle takes a different value. In the former case they are classified as (Zagouras & Markellos, 1977): type (a) if symmetric with respect to the (x, z) plane ($\dot{x}(\bar{X}_0, T) = \dot{x}_0 = 0, \dot{z}(\bar{X}_0, T) = \dot{z}_0 = 0$); or type (B) if symmetric with respect to the x axis ($\dot{x}(\bar{X}_0, T) = \dot{x}_0 = 0, z(\bar{X}_0, T) = z_0 = 0$). Type (a) and type (B) SPOs are also known as F-type and G-type (Kotoulas & Voyatzis, 2005).

It is known that the planar retrograde 1/2 resonance is a 3rd order resonance (Morais & Giuppone, 2012; Morais & Namouni, 2013b). Accordingly, planar periodic orbits associated with the retrograde 1/2 resonance have multiplicity 3, i.e. they intersect the Poincaré map $y = 0$ with the same sign for \dot{y} , 3 times per period (Morais & Namouni, 2013b). Therefore we restrict our search to POs of multiplicity 3. We compute the circular family of POs with the same multiplicity since from this there may be bifurcations to resonant planar POs (Hadjidemetriou, 1988; Kotoulas & Hadjidemetriou, 2002) and 3D POs (Hénon, 1973; Antoniadou & Libert, 2019; Morais & Namouni, 2019; Kotoulas & Voyatzis, 2020b).

The numerical integration of the CR3BP equations of motion and associated variational equations were done using the Bulirsch-Stoer algorithm. Distance and time were scaled by the planet's semimajor axis and orbital period. The computations for an individual test particle were stopped when the distance to a massive body was within its physical radius (taken equal to the Sun's and Jupiter's radius). They were also stopped when the heliocentric distance exceeded 10 times the planet's semi-major axis.

Standard algorithms for computation of POs were used (Zagouras & Markellos, 1977; Howell, 1984; Voyatzis et al., 2018). These consist of a predictor-corrector scheme where: 1) a guess PO, \bar{X}_0 , is followed until the 3rd intersection with the surface of section ($|y| < \epsilon_0$) occurs; 2) the periodicity condition $\|\bar{X} - \bar{X}_0\| < \epsilon$ is checked; 3) if satisfied the PO was found and a nearby guess PO is followed; otherwise a differential correction is applied to the guess PO and the scheme is repeated. Once the PO is found the eigenvalues of the monodromy matrix $\Delta(T)$ are computed in order to decide if it is stable or unstable (Hadjidemetriou, 2006). As the equations of motion are symplectic, $|\Delta(T)| = 1$, hence these eigenvalues appear as reciprocal pairs. They may form real or complex conjugate pairs. One pair of (trivial) eigenvalues is unitary (Hadjidemetriou, 2006). Stability occurs if the other pair(s) are complex conjugate on the unit circle.

For planar POs, 2D and vertical stability indexes may be computed (Hadjidemetriou, 2006; Hénon, 1973). Stable planar periodic orbits have 2D stability index $-2 < k_2 < 2$. Change of stability occurs when $|k_2| = 2$ (i.e. when the non-trivial pair of eigenvalues is real on the unit circle) which is often associated with bifurcation of a new family of POs (Hadjidemetriou, 2006). Motion around stable 2D periodic orbits is maintained when there are small deviations out of the plane only if the vertical stability index $-2 < k_3 < 2$. When $k_3 = 2$ (vertical critical orbit or *vco*) a bifurcation into a new family of 3D periodic orbits with the same multiplicity may occur (Hénon, 1973; Ichtiaroglou & Michalodimitrakis, 1980).

Generally, to find planar and 3D POs, it was sufficient to use double precision arithmetics with parameters $\epsilon_0 = 10^{-13}$ and $\epsilon = 10^{-12}$. To monitor the POs computations we checked that $|\Delta(T)| = 1$ with at least 10 significant digits. Stability was checked by explicitly computing the eigenvalues of $\Delta(T)$ and unstable nearly critical motion (near the transition to stability) was confirmed by computing the chaos indicator MEGNO (Cincotta

& Giordano, 2006). In order to follow the unstable families to termination and to decide on the stability of nearly critical families it was sometimes necessary to use quadruple precision arithmetics.

3 The 2D families and bifurcations into 3D

Morais & Namouni (2013b) showed that the relevant resonant argument for the planar retrograde 1/2 resonance in the CR3BP is $\phi^* = 2\lambda^* + \lambda_p^* - 3\varpi^*$. The modified (retrograde) $*$ angles are related to the standard (prograde) angles by the relations $\lambda^* = \lambda - 2\Omega$, $\lambda_p^* = -\lambda_p$, $\varpi^* = \varpi - 2\Omega = \omega - \Omega$ where λ , Ω , $\varpi = \omega + \Omega$ and ω are the test particle's mean longitude, longitude of ascending node, longitude of pericenter and argument of pericenter, and λ_p is the mean longitude of the planet.¹ Therefore, we may also write $\phi^* = 2\lambda - \lambda_p + 2\Omega - 3\varpi = 2\lambda - \lambda_p - \Omega - 3\omega$. Note that D'Alembert rule is obeyed when using either modified or standard angles.

3.1 Planar POs

There are 2 planar resonant modes, corresponding to the libration centers: $\phi^* = 0$ when the pericenter is interior and at conjunction (aligned) with the planet's orbit; $\phi^* = 180^\circ$ when the pericentre is interior or exterior and at opposition (anti-aligned) with the planet's orbit (Morais & Namouni, 2013b, 2016b).

We show how the planar families of symmetric POs (SPOs) evolve with the Jacobi constant, C , in Fig. 1 (resonant mode with $\phi^* = 0$) and Fig. 2 (circular family and resonant mode with $\phi^* = 180^\circ$).

The eccentric family (named R_{Ib} in Kotoulas & Voyatzis (2020b)) is horizontally stable except for a barely visible small segment at the start near collision with the planet. This family corresponds to the resonance center $\phi^* = 0$. There is a *vco* at $C = -1.5649$ and 3D quasiperiodic orbits around the family exist when $C > -1.5649$. The family occurs above the pericentric collision line with the planet (Morais & Namouni, 2016b), and ends by collision with the star. We call this the high eccentricity resonant mode.

The circular family, when computed with multiplicity 3, is vertically stable with a single *vco* at $C = -1.8924$. At $C = -1.8895$ (where the ratio of mean motions is very close to 1/2) the horizontal stability index on the circular family reaches the value $k_2 = 2$ and a bifurcation into a pair of stable / unstable POs occurs. The unstable branch corresponds to $\phi^* = 0$ (family R_{Ia} in Kotoulas & Voyatzis (2020b)). The stable branch corresponds to the resonant mode $\phi^* = 180^\circ$ (family R_{IIa} in Kotoulas & Voyatzis (2020b)) and is horizontally stable from the bifurcation when $e \approx 0$ up to $C = -0.7505$ (when $e \approx 0.8$) near collision with the planet which occurs midway between apocentre and pericentre (Morais & Namouni, 2016b). When $C > -0.7505$ the family is horizontally unstable and when $C > -0.5286$ it is also vertically unstable. At $C = -0.7505$ and $C = -0.5286$ the stability indexes are $k_2 = -2$ and $k_3 = -2$, respectively. Associated possible bifurcation into 2D and 3D families with multiplicity 6 are very difficult to confirm due to the strong chaos that exists at these locations. Note that the stable family which exists up to eccentricity

¹ Morais & Namouni (2013b) showed that the retrograde resonant angles may be obtained from the standard prograde disturbing function by applying a canonical transformation $\lambda_p^* = -\lambda_p$, $\omega^* = \omega - \pi$, $\Omega^* = -\Omega - \pi$ which is equivalent to inverting the planet's motion hence swapping ascending and descending nodes.

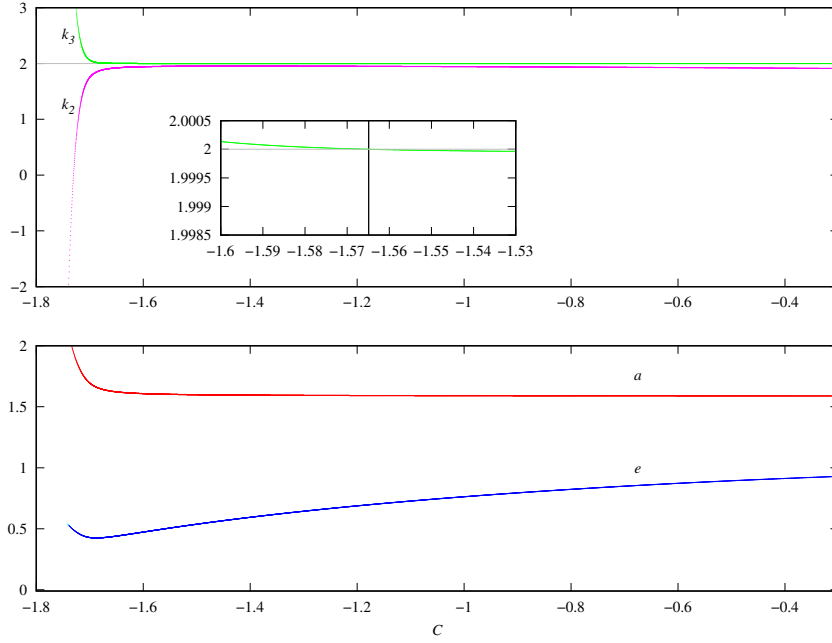


Fig. 1 The SPO family corresponding to the resonance center $\phi^* = 0$. Top panel: 2D (magenta) and 3D (green) stability indexes with zoom of vco . The black vertical line in the zoom panel locates the vco . Low panel: semi-major axis a and eccentricity e (horizontally stable (red / blue)).

nearly 1 at Neptune to Sun mass ratio (named R_{IIb} in Kotoulas & Voyatzis (2020b)) does not occur at Jupiter to Sun mass ratio.

3.2 Periodic orbits in 3D

As shown by Namouni & Morais (2020b) in the 3-dimensional case the relevant resonant angles are $\phi_k = 2\lambda - \lambda_p - \Omega - k\omega$, where ω is the argument of pericenter and k is an odd integer for the 1/2 resonance. When $k = 1$ we have the planar prograde angle $\phi_1 = \phi = 2\lambda - \lambda_p - \Omega - \omega$ and when $k = 3$ we have the planar retrograde angle $\phi_3 = \phi^* = 2\lambda - \lambda_p - \Omega - 3\omega$, respectively. Recall that when using the modified (retrograde) angles from Morais & Namouni (2013b) we have $\phi = 2\lambda^* + \lambda_p^* - \varpi^* + 2\Omega$ and $\phi^* = 2\lambda^* + \lambda_p^* - 3\varpi^*$. These modified angles are part of a canonical set of variables adequate to study retrograde resonance. Particularly, they give us information about retrograde resonance structure: ϕ is associated with a mixed type 3rd order resonance (Namouni & Morais, 2015) while ϕ^* is associated with an eccentricity 3rd order resonance (Morais & Namouni, 2013b).

The planar SPOs from the previous section may be continued into 3-dimensional SPOs starting at the vco s which occur at: $C = -1.8924$ (circular family); $C = -1.5649$ and $e = 0.4966$ (resonant family corresponding to $\phi^* = 0$). In general, SPOs correspond to the resonant centers 0 or 180° . The 1/2 resonance may also have asymmetric periodic orbits (APOs) which correspond to resonant centers different from 0 and 180° (Voyatzis et al., 2018), (Namouni & Morais, 2020b).

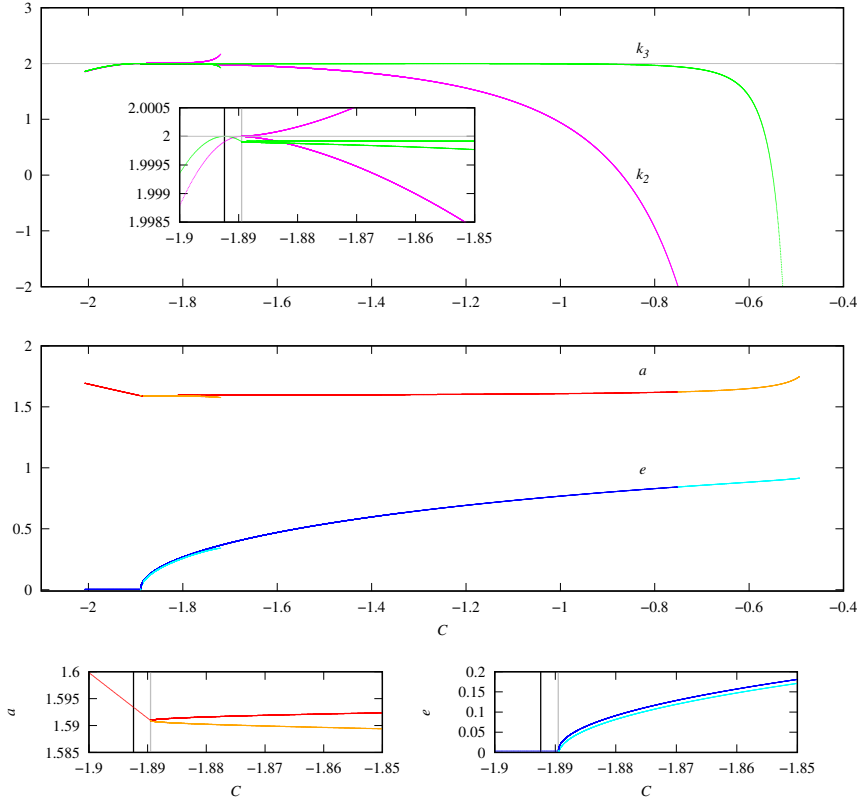


Fig. 2 The nearly circular SPO family and its bifurcations into a stable family (corresponding to the resonance center $\phi^* = 180^\circ$) and an unstable family (corresponding to $\phi^* = 0$). Top panel: 2D (magenta) and 3D (green) stability indexes with zoom of *vco* and 2D bifurcation. Middle panel: semi-major axis *a* and eccentricity *e* (horizontally stable (red / blue) and unstable (orange / cyan)). Low panel: zoom of bifurcation region. Vertical lines in the zoom panels locate the *vco* (black line) and the 2D bifurcation of the circular family into a stable / unstable pair (gray line).

Figure 3 shows the 3D SPOs bifurcating from the *vcos* on the planar families. There are 2 symmetric families bifurcating from the *vco* at $C = -1.8924$ on the circular family. One has type (a) or F symmetry and is initially stable but changes stability at $C = -1.5545$ (clearly seen in Fig. 3 bottom right panel) which corresponds to the maximum value of the Jacobi constant. The other has type (B) or G symmetry and is always unstable but initially nearly critical due to the proximity to the *vco*. Kotoulas & Voyatzis (2020b) identify a similar bifurcation when using a Neptune to Sun mass ratio, into type (a) and type (B) SPOs which they classify as R01 and R0G families. Continuation of the type (a) family shows that it connects to the *vco* at $C = -1.5649$ on the 2D family corresponding to the resonant mode $\phi^* = 0$, similarly to the case with Neptune to Sun mass ratio (Kotoulas & Voyatzis 2020 b). However, note that in the latter case no change of stability along the family was detected.

The type (a) SPO family which bifurcates from the nearly circular family, initially corresponds to the fixed point of the resonance Hamiltonian with $\phi = 0$, $\omega = 270^\circ$ i.e. $\phi^* = 180^\circ$. The eccentricity along the family decreases until the value zero is reached

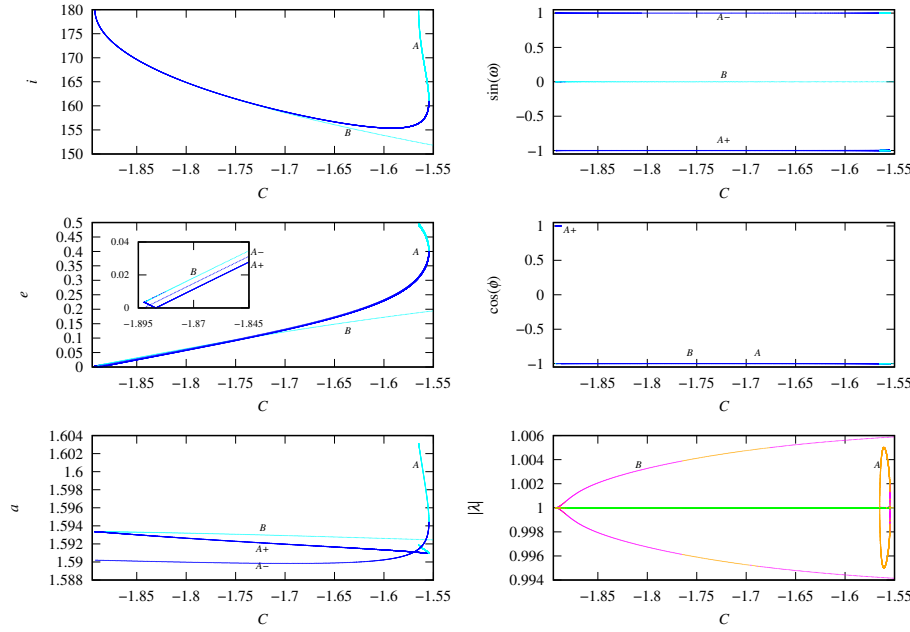


Fig. 3 Families of 3D symmetric periodic orbits bifurcating from the v_{cos} . Left panels: inclination i ; eccentricity e with zoom; semi-major axis a . Right panels: cosine of argument of pericenter ω ; cosine of prograde resonant angle $\phi = \phi_1$; eigenvalues amplitudes $|\lambda|$. The families are coloured blue (cyan) when stable (unstable). There are 2 families bifurcating from the v_{co} on the circular planar family. One has type (a) symmetry, is initially stable (complex conjugate eigenvalues with unit amplitude), becomes unstable but nearly critical at $C = -1.5545$ (one pair of real eigenvalues with unit amplitude) and ends at the v_{co} on the resonant eccentric planar family. The other has type (B) symmetry and is unstable but initially nearly critical (one pair of real reciprocal eigenvalues with amplitudes close to unit). The families are labeled b (unstable type (B)) and a (type (a)). The branches labeled $a+$ and $a-$ refer to distinct intersections of the type (a) family with the surface of section which are obtained by continuation from the v_{cos} at $C = -1.8924$ and $C = -1.5649$, respectively.

and then increases again (Fig. 3, middle left). At this point there is a shift to the fixed point with $\phi = 180^\circ$, $\omega = 270^\circ$ i.e. $\phi^* = 0$ (Fig. 3, top & middle right). This change of topology is reproduced in our Hamiltonian model for 3D retrograde resonance described in the next section. Continuation from the v_{co} at $C = -1.5649$ retrieves the same family but at a different intersection with the surface of section which corresponds to the fixed point of the resonance Hamiltonian with $\phi = 180^\circ$, $\omega = 90^\circ$ i.e. $\phi^* = 0$ (Fig. 3, top & middle right). In Fig 3, the labels $a+$ and $a-$ are used to distinguish the 2 intersections of the (a) type family with the surface of section. Examples of POs on the sections $a+$ and $a-$ are shown in Fig. 4 (top left and right panels). On the unstable nearly critical branch bifurcating from the v_{co} at $C = -1.5649$ on the resonant family, $\phi^* = 0$ with ω circulating on several thousand years timescale around the Kozai centers at $\omega = 0, 180^\circ$ (Fig. 4, bottom left panel). Near the transition to stability at $C = -1.5545$, MEGNO increases linearly with time at a slow rate (Fig. 4, bottom left panel). MEGNO converges to 2 on the family's stable branch since motion is regular (Fig. 4, top panels).

The type (B) SPO corresponds to the unstable fixed points $\phi = 180^\circ$, $\omega = 0, 180^\circ$ (Fig. 3, top & middle right). After several thousand years, there is alternating libration

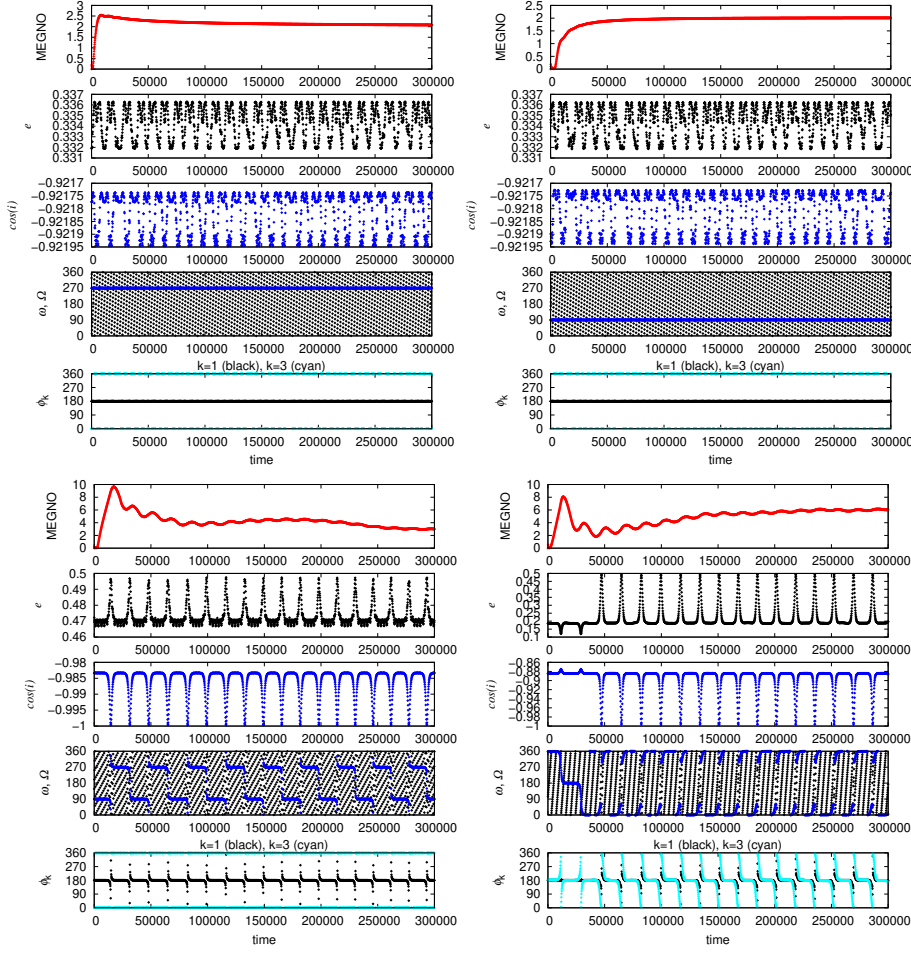


Fig. 4 Top panels: Type (a) SPOs at $C = -1.5600$ (stable branches originating from bifurcations from the v_{cos} on the circular family (left) and resonant family corresponding to $\phi^* = 0$ (right)). Low left panel: Type (a) SPO at $C = -1.5600$ (unstable nearly critical branch). Low right panel: Type (B) SPO at $C = -1.5600$. From top to bottom panels: MEGNO; eccentricity, cosine of inclination, argument of pericenter ω (blue) and longitude of ascending node Ω (black); resonant angles $\phi = \phi_1$ (black) and $\phi^* = \phi_3$ (cyan).

and circulation around $\omega = 90^\circ, 270^\circ$ which indicates the presence of Kozai separatrices (Fig. 4, bottom right panel) with typical coupled eccentricity and inclination oscillations. Again MEGNO increases linearly with time indicating chaotic diffusion.

The connection between the 2 families becomes clearer when plotting the orbits' evolution in Kozai-type (e, ω) diagrams (Fig. 5). While the stable type (a) SPO family corresponds to the Kozai centers at $\omega = 90^\circ, 270^\circ$ (blue), the unstable but nearly critical type (B) SPO family evolves towards Kozai separatrices around these centers (black). At $C = -1.8500$ the unstable nearly critical type (B) SPO overlaps with the stable centers corresponding to the type (a) SPO family while at $C = -1.6000$ and $C = -1.5600$ the 2 families are well separated. At $C = -1.5600$ the unstable nearly critical type (B) SPO

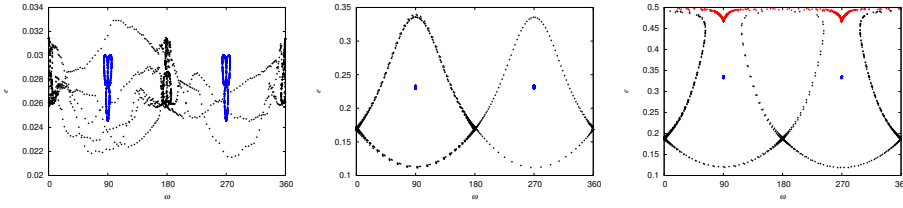


Fig. 5 Kozai diagrams for type (B) SPO (black), stable type (a) SPOs (blue) and nearly critical type (a) SPO (red) at $C = -1.8500$ (left), $C = -1.6000$ (middle) and $C = -1.5600$ (right). Evolution of the orbits over 3×10^5 planet's periods.

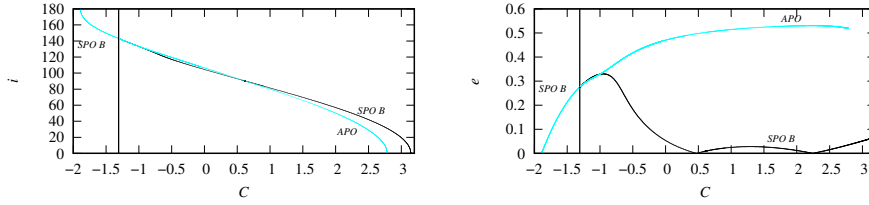


Fig. 6 The bifurcation of the type (B) symmetric family (*SPO B*) into an single unstable asymmetric family (*APO*) and a double unstable symmetric family (*SPO B*). Left panel: inclination i . Right panel: eccentricity e . The black vertical line indicates the bifurcation at $C \approx -1.308$. The colours cyan/black indicate if the family is single unstable (one λ_i larger than 1) or double unstable (two λ_i larger than 1).

corresponding to $\phi = 180^\circ$ connects with the nearly critical branch on the type (a) SPO corresponding to $\phi^* = 0$ and circulation around the Kozai centers at $\omega = 0, 180^\circ$ (red).

The type (a) SPO family exists in the range $-1.8924 < C < -1.5545$. When $C > -1.5545$ only the type (B) SPO family persists. Instability, measured by the maximum eigenvalues' amplitudes, increases with C (Fig. 3 bottom right). At $C \approx -1.308$ the family divides into 2 branches of POs with different properties which could be continued to $i = 0$ (Fig. 6). One branch corresponds to the SPO type (B) family which becomes double unstable (two eigenvalues' amplitudes, $|\lambda|$, larger than 1) at the bifurcation point. This branch connects with the prograde A_2 family from Kotoulas & Hadjidemetriou (2002). The 2nd branch is single unstable (one eigenvalue amplitude, $|\lambda|$, larger than 1) asymmetric and corresponds to the continuation of family A_{22} identified in the prograde problem by Voyatzis et al. (2018).

4 Resonance capture in 2D and 3D

We simulate resonant capture following the setup in Namouni & Morais (2015, 2017). Stoke's drag causes the test particle's semimajor axis to drift towards the resonance following an exponential decay law $a = a_0 \exp^{-t/\tau}$. We ensure adiabatic capture by choosing a long characteristic decay time $\tau = 10^7$ planet's periods.

In the planar problem, outer orbits slowly approaching the planet follow the nearly circular non-resonant family which bifurcates into a resonant SPO corresponding to $\phi^* = 180^\circ$. However, capture in the 1/2 retrograde resonance never occurs for planar circular orbits. As shown by (Morais & Giuppone, 2012; Morais & Namouni, 2013b), the resonant term is

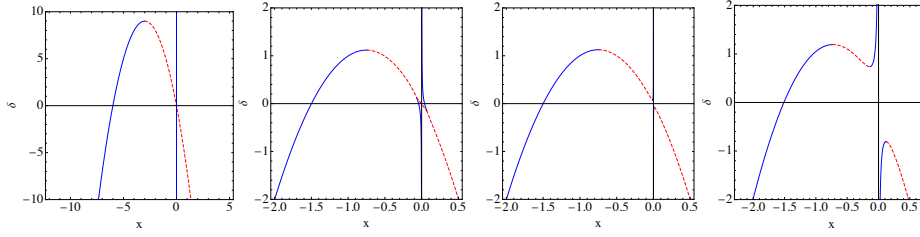


Fig. 7 Bifurcation diagrams of the Hamiltonians for retrograde 3rd order resonance: 2D case from Morais & Giuppone (2012) with $H = \delta(x^2 + y^2)/2 + (x^2 + y^2)^2/4 - 2x(x^2 - 3y^2)$ and $x \propto e^3 \cos \phi_3$ (left); 3D case from Namouni & Morais (2015) with $H = (\delta + 2x)(x^2 + y^2) + (x^2 + y^2)^2 + xT$ and $x \propto e \cos^2(i/2) \cos \phi^*$, $T = -0.01$ (middle left) $T = 0.001$ (middle right) and $T = 0.1$ (right). The parameter $\delta \propto n_p - 2n$ decreases as the particle drifts towards resonance, while T is a proxy for $(\pi - i)^2 - 2e^2$. Stable (unstable) fixed points are shown in solid blue (dashed red). The vertical line locates $x = 0$.

$e^3 \cos \phi^*$. The equilibrium points of an Hamiltonian model for this planar 3rd order resonance valid at small to moderate eccentricities (Murray & Dermott, 1999) are shown in the bifurcation diagram (x, δ) , where $x \propto e^3 \cos \phi^*$ and $\delta \propto n_p - 2n$ (Fig. 7 left). When exact resonance ($\delta = 0$) is reached, the unstable fixed point is at $e = 0$. Therefore, the final outcome will always be ϕ^* circulating outside the resonant separatrix.

3D nearly circular outer orbits drifting towards the planet are 1st captured in the resonant mode $\phi = 180^\circ$. In Namouni & Morais (2015) we explained this with an Hamiltonian model of the mixed resonance, $e \cos^2(i/2) \cos \phi$, which has an additional parameter, T , a proxy for $(\pi - i)^2 - 2e^2$. In Fig. 7 we show the corresponding bifurcation diagrams (x, δ) where $x \propto e \cos^2(i/2) \cos \phi$, for different values of T . Before resonance passage ($\delta > 0$) when $T > 0$ there are 3 apocentric ($x < 0$, i.e. corresponding to $\phi = 180^\circ$) equilibrium points: 2 stable and 1 unstable, but as resonance ($\delta = 0$) is approached only the higher eccentricity stable apocentric equilibrium (branch on the left) remains (Fig. 7 right), similar to a 1st order resonance. Therefore, capture in $\phi = 180^\circ$ occurs with 100% probability. Indeed, we confirmed numerically that this occurs when $i \leq 174.7^\circ$. As the inclination increases, the parameter T decreases and the unstable apocentric equilibrium moves closer to $x = 0$ (Fig. 7 middle right). When $T = 0$ the topology of the 3rd order mixed resonance is similar to that of the eccentricity resonance (Fig. 7 left): the unstable fixed point is exactly at $x = 0$ when $\delta = 0$. When the inclination approaches 180° , T becomes slightly negative (Fig. 7 middle left) and when $\delta > 0$ the stable equilibrium at small eccentricity has $x > 0$ (pericentric i.e. corresponding to $\phi = 0$) in agreement with the behaviour at the start of the type (A) SPO family described in the previous section. Since the unstable equilibrium is always near $x = 0$, capture in resonance never occurs for nearly circular orbits with $i > 174.7^\circ$.

A typical example of 3D capture with $a_0 = 1.8$, $e = 0$, $i = 170^\circ$ is shown in Fig. 8 (top left). At $C \approx -1.856$ there is capture in $\phi = 180^\circ$ with an increase of eccentricity and decrease of inclination characteristic of a mixed type $e \cos^2(i/2) \cos \phi$ resonance. At $C \approx -1.604$ there is Kozai libration around $\omega = 90^\circ$ with large coupled oscillations in eccentricity and inclination which lead to capture in $\phi^* = 0$ at $C \approx -1.562$ when $e > 0.4$, with an associated increase of eccentricity characteristic of an eccentricity $e^3 \cos \phi^*$ resonance. This 3-stage capture mechanism was first observed in the numerical simulations from Namouni & Morais (2015) and occurs for nearly circular orbits with $175^\circ \gtrsim i \gtrsim 155^\circ$.

We follow initial conditions on the SPO families to understand their role in resonant capture. At $C = -1.8500$ the evolution of initial conditions on the type (A) and type (B)

families are indistinguishable, due to their proximity (Fig. 5, left). The presence of dissipation implies that there is a drift from the stable resonance centers associated with the type (A) family and the test particle follows the typical capture path as if it was started on the unstable nearly critical type (B) family (Fig. 8 top right). At $C = -1.6000$ the 2 families are now separated hence the test particle remains on the type (A) SPO family which corresponds to the fixed point $\phi = 180^\circ$, $\omega = 270^\circ$ and $\phi^* = 0$ (Fig. 8 bottom left), with eccentricity and inclination increasing as C increases due to dissipation. At $C = -1.5545$, a saddle-node bifurcation occurs on the type (A) SPO family (Fig. 3) but the eccentricity is large enough for capture in a 3D quasiperiodic orbit around the 2D resonant mode $\phi^* = 0$. The initial condition on the type (B) family at $C = -1.6000$ (Fig. 8 bottom right) evolves towards the Kozai separatrix around the centers $\omega = 90^\circ, 270^\circ$ on the type (A) family, with typical coupled oscillations of eccentricity and inclination. The eccentricity of these Kozai centers increases as the semi-major axis decreases. Once the saddle-node bifurcation on the type (A) SPO family occurs at $C = -1.5545$, there is capture in a 3D quasiperiodic orbit around the 2D resonant mode $\phi^* = 0$ which is vertically stable when $C > -1.5649$.

Additional information on the topology of the 1/2 retrograde resonance may be obtained by integrating orbits in (a, i) grids at set initial values of e , ω and ϕ . In Fig. 9 we show examples of grid integrations over 5×10^6 binary periods with $\omega = 90^\circ$, $\phi = 180^\circ$ (thus $\phi^* = 0$), $e = 0.1$ (left) and $e = 0.3$ (right). The lower panels show zooms of the upper panels around the fixed points which correspond to the stable branch of the type (A) SPO. The regions of ϕ libration around 180° (marked with circles) and ϕ^* libration around 0 (marked with triangles) connect. The type (A) SPO (marked by the overlap of circles, triangles and + signs, better observed in the lower panels) is surrounded by quasiperiodic orbits such that ϕ librates around 180° . Due to the proximity between the two SPO families, the set of quasiperiodic orbits with ϕ librating around 180° such that ω circulates is dominant over the set where ω librates around the Kozai center 90° . We confirmed numerically that, when Stoke's drag is included, initial conditions corresponding to these quasiperiodic islands may be captured directly in the $\phi^* = 0$ resonant mode due to the increase in eccentricity which occurs during the $\phi = 180^\circ$ mixed-resonance stage. Note that the stable center corresponding to the type (A) SPO family is better defined on the right panel ($e = 0.3$) than on the left panel ($e = 0.1$) when the stable and unstable families nearly overlap.

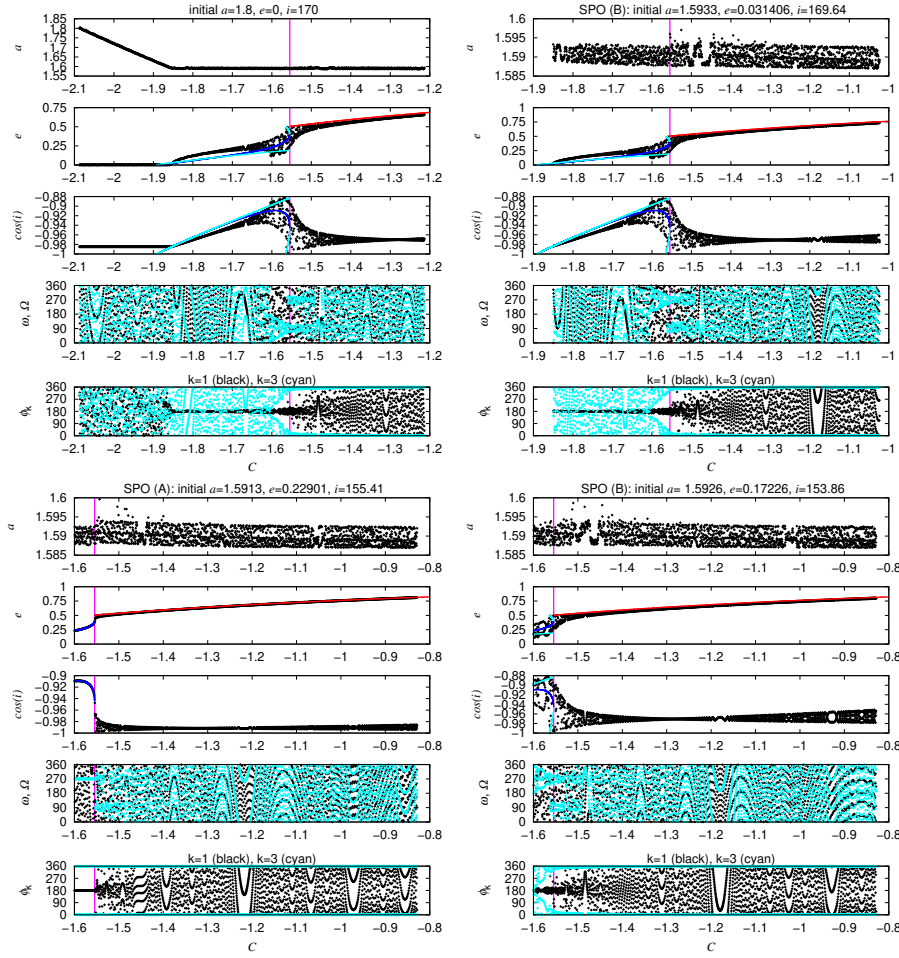


Fig. 8 Evolution of orbits subject to Stokes' drag (semimajor axis exponential decay law with characteristic time $\tau = 10^7$ planet's periods). Top left: initial $a = 1.8$, $e = 0$, $i = 170^\circ$. Top right: initially at the SPO type (A) or type (B) family with $C = -1.8500$. Bottom left / right: initially on the type (A) / type (B) family with $C = -1.6000$. From top to bottom panels: semi-major axis; eccentricity, cosine of inclination, argument of pericenter ω (blue) and longitude of ascending node Ω (black); resonant angles $\phi = \phi_1$ (black) and $\phi^* = \phi_3$ (cyan).

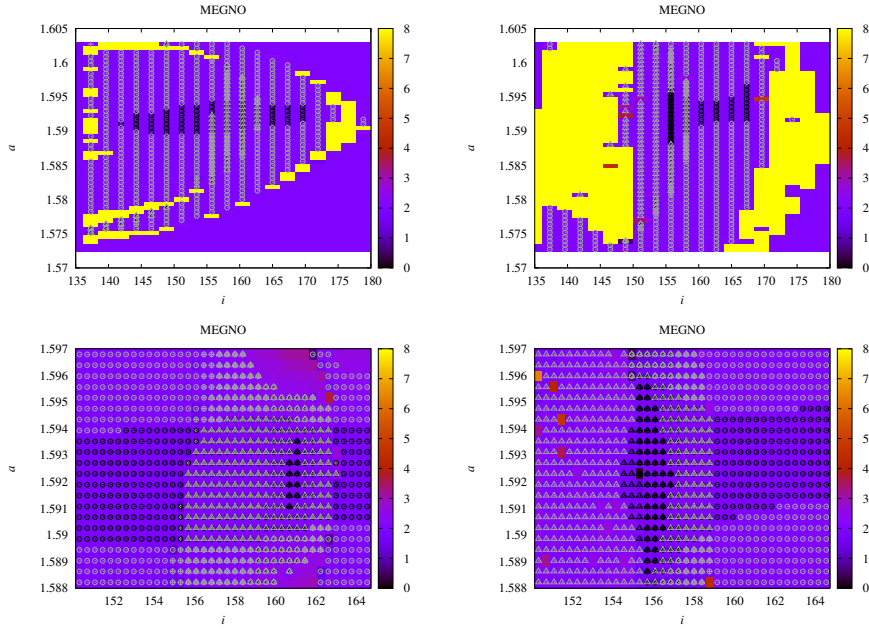


Fig. 9 MEGNO maps (color scale) for 1/2 retrograde resonance with initial conditions $\omega = 90^\circ$, $\phi = 180^\circ$ and $\Omega = 0$ (thus $\phi^* = 0$), $e = 0.1$ (left) and $e = 0.3$ (right). Symbols indicate libration of the angles ϕ around 180° (circles), ϕ^* around 0 (triangles) and ω around 90° (+ sign). Overlap of circles, triangles and + signs correspond to orbits with all angles librating (inside the separatrix). Black (gray) symbols indicate libration amplitude less (larger) than 50° . The lower panels are zooms of the upper panels around the fixed points which correspond to the stable branch of the type (A) SPO family.

5 Conclusion

We continued our work on resonant capture in 3D (Namouni & Morais, 2015, 2017, 2018b) and the relation with the PO families (Morais & Namouni, 2019).

We obtained the families of POs associated with the 1/2 retrograde resonance at Jupiter to Sun mass ratio. The planar resonant POs correspond to $\phi^* = 180^\circ$ which bifurcates from the circular family, and $\phi^* = 0$ which we call the high eccentricity resonant family since it exists only above the pericentric collision line at $e > 0.4$. A family of type (A) SPOs bifurcates from the $vcos$ on the circular family and on the resonant $\phi^* = 0$ family. The stable branch of the type (A) SPO family corresponds to a stable fixed point of the averaged (resonant) Hamiltonian with $\phi = 180^\circ$ and $\omega = 90^\circ, 270^\circ$ (thus $\phi^* = 0$).

There is a type (B) SPO family also bifurcating from the vco on the circular family which is unstable but initially nearly critical and corresponds to the libration center $\phi = 180^\circ$. When inclination is close to 180° the two SPO families nearly overlap. Due to this proximity, when a small adiabatic dissipation akin to Stoke's drag is included, the orbit follows the nearly critical type (B) family with $\phi = 180^\circ$. Slow chaotic diffusion on the type (B) SPO causes Kozai oscillations around the centers $\omega = 90^\circ, 270^\circ$ which correspond to the stable branch of the type (A) SPO. As the semi-major axis decreases due to dissipation these Kozai centers are displaced to larger eccentricity and there is capture into a quasiperiodic orbit associated with the resonant mode $\phi^* = 0$. This capture is possible once a critical value of the Jacobi constant (associated with a saddle-node bifurcation on the type (A) SPO family) is reached.

In the case of the 1/2 resonance (studied here) and the 1/1 resonance (Morais & Namouni, 2019), 3D SPOs bifurcating from the $vcos$ on the circular family and on the high eccentricity resonant family connect. In 3D, at small eccentricity, there is libration of the prograde resonant angle ϕ around 180° . When slow dissipation is included these orbits evolve towards Kozai separatrices. Kozai libration is extended in the case of the 1/2 resonance as it is associated with an unstable but nearly critical family and not just a single PO as for the 1/1 resonance. In both cases, there is chaotic drift on Kozai separatrices and the displacement of the Kozai centers at $\omega = 90^\circ, 270^\circ$ to larger eccentricity. Capture in a 3D quasiperiodic orbit around the high eccentricity retrograde resonant mode occurs at a critical point, connecting the stable and unstable branches bifurcating from the $vcos$ on the circular and resonant high eccentricity families, respectively.

Stable PO families are the likely end states for dynamical systems. However, computation of stable POs does not provide information about the extent of quasiperiodic orbits around them. Here, we showed that in the presence of slow dissipation, unstable but nearly critical POs mediate transitions between distinct stable families. Combining computation of PO families with stability maps based on a chaos indicator is useful in order to gain insight into the extent of the quasiperiodic orbits around a PO family and the role played by unstable but nearly critical families which exhibit slow and sticky chaotic diffusion (Zaslavsky, 2007).

Acknowledgments

Bibliography access was provided by CAPES-Brazil. M.H.M. Morais research had financial support from São Paulo Research Foundation (FAPESP/2018/08620-1) and CNPQ-Brazil (PQ2/304037/2018-4).

References

- Antoniadou K. I., Libert A.-S., 2019, *Mon. Not. R. Astron. Soc.* , 483, 2923
- Antoniadou K. I., Voyatzis G., 2014, *Astrophysics and Space Science*, 349, 657
- Cincotta P. M., Giordano M., 2006
- Gayon J., Bois E., 2008, *Astron. Astrophys.* , 482, 665
- Gayon-Markt J., Bois E., 2009, *Mon. Not. R. Astron. Soc.* , 399, L137
- Hadjidemetriou J. D., 1988, *Celestial Mechanics*, 43, 371
- Hadjidemetriou J. D., 2006, p. 43
- Hénon M., 1973, *Celestial Mechanics*, 8, 269
- Howell K. C., 1984, *Celestial Mechanics*, 32, 53
- Ichtiaroglou S., Michalodimitrakis M., 1980, *Astron. Astrophys.* , 81, 30
- Kotoulas T., Voyatzis G., 2020a, *Plan. Space Sci.* , 182, 104846
- Kotoulas T., Voyatzis G., 2020b, *Celestial Mechanics and Dynamical Astronomy*, 132, 33
- Kotoulas T. A., Hadjidemetriou J. D., 2002, *Earth Moon and Planets*, 91, 63
- Kotoulas T. A., Voyatzis G., 2005, *Astron. Astrophys.* , 441, 807
- Li D., Mustill A. J., Davies M. B., 2019, *Mon. Not. R. Astron. Soc.* , 488, 1366
- Morais M. H. M., Giuppone C. A., 2012, *Mon. Not. R. Astron. Soc.* , 424, 52
- Morais M. H. M., Namouni F., 2013a, *Mon. Not. R. Astron. Soc.* , 436, L30
- Morais M. H. M., Namouni F., 2013b, *Celestial Mechanics and Dynamical Astronomy*, 117, 405
- Morais M. H. M., Namouni F., 2016a, *Celestial Mechanics and Dynamical Astronomy*, 125, 91
- Morais M. H. M., Namouni F., 2016b, *Comp. Appl. Math.*, 35, 881–891
- Morais M. H. M., Namouni F., 2017, *Nature*, 543, 635
- Morais M. H. M., Namouni F., 2019, *Mon. Not. R. Astron. Soc.* , 490, 3799
- Murray C. D., Dermott S. F., 1999, *Solar system dynamics*. Cambridge University Press
- Namouni F., Morais M. H. M., 2015, *Mon. Not. R. Astron. Soc.* , 446, 1998
- Namouni F., Morais M. H. M., 2017, *Mon. Not. R. Astron. Soc.* , 467, 2673
- Namouni F., Morais M. H. M., 2018a, *Mon. Not. R. Astron. Soc.* , 477, L117
- Namouni F., Morais M. H. M., 2018b, *J. Comp. App. Math.*, 37, 65
- Namouni F., Morais M. H. M., 2018c, *Mon. Not. R. Astron. Soc.* , 474, 157
- Namouni F., Morais M. H. M., 2020a, *Mon. Not. R. Astron. Soc.* , 494, 2191
- Namouni F., Morais M. H. M., 2020b, *Mon. Not. R. Astron. Soc.* , 493, 2854
- Voyatzis G., Tsiganis K., Antoniadou K. I., 2018, *Celestial Mechanics and Dynamical Astronomy*, 130, 29
- Wiegert P., Connors M., Veillet C., 2017, *Nature*, 543, 687
- Zagouras C., Markellos V. V., 1977, *Astron. Astrophys.* , 59, 79
- Zaslavsky G. M., 2007, *The Physics of Chaos in Hamiltonian Systems*. World Scientific. Singapore